

# TRIS I : Absolute Measurements of the Sky Brightness Temperature at 0.6, 0.82 and 2.5 GHz

M. Zannoni<sup>1</sup>, A. Tartari, M. Gervasi<sup>1,2</sup>, G. Boella<sup>2</sup>, G. Sironi<sup>1</sup>,  
A. De Lucia and A. Passerini

*Physics Department, University of Milano Bicocca, P.zza della Scienza 3, I20126 Milano  
Italy*

F. Cavaliere

*Physics Department, University of Milano, via Celoria 16, I20133 Milano Italy*

mario.zannoni@mib.infn.it

## ABSTRACT

At frequencies close to 1 GHz the sky diffuse radiation is a superposition of radiation of Galactic origin, the 3 K Relic or Cosmic Microwave Background Radiation, and the signal produced by unresolved extragalactic sources. Because of their different origin and space distribution the relative importance of the three components varies with frequency and depends on the direction of observation. With the aim of disentangling the components we built TRIS, a system of three radiometers, and studied the temperature of the sky at  $\nu = 0.6$ ,  $\nu = 0.82$  and  $\nu = 2.5$  GHz using geometrically scaled antennas with identical beams (HPBW =  $18^\circ \times 23^\circ$ ). Observations included drift scans along a circle at constant declination  $\delta = +42^\circ$  which provided the dependence of the sky signal on the Right Ascension, and absolute measurement of the sky temperature at selected points along the same scan circle. TRIS was installed at Campo Imperatore (lat. =  $42^\circ 26'$  N, long. =  $13^\circ 33'$ , elevation = 2000 m a.s.l.) in Central Italy, close to the Gran Sasso Laboratory.

*Subject headings:* diffuse radiation, galactic emission, cosmic microwave background, unresolved extragalactic sources, sky absolute temperature

---

<sup>1</sup>also Italian National Institute for Astrophysics, INAF, Milano.

<sup>2</sup>also Italian National Institute for Nuclear Physics, INFN, Milano-Bicocca.

## 1. Introduction

The diffuse radiation from the sky is a superposition of components. At frequencies between few tens of MHz and few tens of GHz, in terms of brightness temperature we can write

$$T_{sky}(\alpha, \delta, \nu) = T_{gal}(\alpha, \delta, \nu) + T_{CMB}(\nu) + T_{uers}(\nu) \quad (1)$$

where  $\alpha$  and  $\delta$  are the Right Ascension and declination of the point at which the telescope axis is aimed.  $T_{gal}$  is the Galactic contribution: partially polarized, anisotropically distributed, it tracks the Galactic structure. Its frequency spectrum is a power law

$$T_{gal}(\nu, \alpha, \delta) = K(\alpha, \delta) \nu^{-\beta(\alpha, \delta)} \quad (2)$$

with spectral index  $\beta$  ranging from 2.1 to 3.4 depending on the relative weight of thermal and synchrotron emission, on the energy spectrum of the Cosmic Ray Electrons and on the Galactic Magnetic Field. Compared to the other components of the diffuse radiation it is a foreground and dominates the sky at frequencies below  $\sim 1$  GHz.

$T_{CMB}$  is the Cosmic Microwave Background. Relic of the Big Bang, it is substantially unpolarized and isotropically distributed. Its flat frequency spectrum is consistent with the emission of a blackbody with a temperature of  $(2.725 \pm 0.001)$  K (Fixsen & Mather 2002). Compared to the other components it is a true background. At  $\nu \geq 1$  GHz  $T_{CMB}$  definitely overcomes  $T_{gal}$  and dominates the sky up to  $\nu \sim 100$  GHz, above which thermal emissions from an irregular distribution of dust with physical temperature  $\geq 20$  K, gradually overwhelms the other components.

$T_{uers}$  is a blend of unresolved extragalactic radio sources isotropically distributed. Its frequency spectrum is a power law

$$T_{uers} = K_{uers} \nu^{-\gamma_{uers}} \quad (3)$$

with  $\gamma_{uers} \sim 2.70$  (Gervasi et al. 2008b).

Each of the above components carries important astrophysical and/or cosmological information, particularly at decimetric wavelengths. At these frequencies for instance we can expect a dip in the flat spectrum of  $T_{CMB}$ , whose detection can provide direct information on  $\Omega_b$  (Burigana et al. 1991), the Universe baryon density. In this same region the slope of the power law frequency spectrum of  $T_{gal}$  changes, revealing perhaps a knee in the energy spectrum of the cosmic ray electrons responsible for the galactic synchrotron radiation. To disentangle these components, coordinated, multifrequency observations of extended areas of sky are necessary. They will form a data base from which the desired information can be extracted modelling the components and optimizing the model parameters. At frequencies

close to 1 GHz it is possible to find in literature maps of  $T_{sky}$  which cover all the sky or large parts of it (see Table 1). Their accuracy is however insufficient to answer many of the questions put forth by present day astrophysical and cosmological models. These maps have been in fact obtained combining data collected at different sites and/or at different times and frequently show artificial structures, e.g. *stripes*. Once *destriped* (see for instance (Platania et al. 2003)), these maps can be used to extract the spectral index of the galactic signal  $T_{gal}$ . The accuracy of the zero level of the absolute scale of temperature of the same maps is however still insufficient to disentangle the radiation components with the accuracy today required by cosmology. To overcome this difficulty we made absolute and differential measurements of the diffuse radiation at three frequencies, using a set of three radiometers (therefore the project is said TRIS), at 0.6, 0.82 and 2.5 GHz. In this paper we present results of these observations. In (Gervasi et al. 2008a) and (Tartari et al. 2008) (from now on cited as Paper II and III), the astrophysical and cosmological implications of TRIS data are discussed.

## 2. Absolute measurements of temperature

Measuring the absolute value of the *brightness temperature*,  $T_{sky}$ , of a patch of diffuse radiation is a conceptually simple but not easy task. Large systematic effects are in fact expected.

A radiometer aimed at the sky gives the *antenna temperature*,  $T_a$ , from which we obtain

$$T_{sky} = \frac{T_a - T_{atm} - T_{env}}{1 - (T_{atm}/T_{atm}^0)} \quad (4)$$

where  $T_{atm}$  and  $T_{env}$  are the noise temperatures of the signals from the atmosphere and the environment above and around the radiometer and  $T_{atm}^0 \simeq 240K$  is the physical temperature of the atmosphere (US Standard Atmosphere 1976). References for calculations are presented in the following Section 4.3.1.

Since the diffuse radiation fills the antenna beam, the absolute value of  $T_a$  is

$$T_a = T_{cold}^{eff} + (S_{sky} - S_{cold})G \quad (5)$$

where

$$G = \frac{T_{warm}^{eff} - T_{cold}^{eff}}{S_{warm} - S_{cold}} \quad (6)$$

is the system *gain* or *conversion factor* and  $S_{sky}$ ,  $S_{cold}$  and  $S_{warm}$  are the radiometer outputs produced by the sky target and by two known sources (*calibrators*), a *cold* and a *warm* load.

$T_x^{eff}$ , the *effective temperature* of calibrator  $x$ , is the convolution of the calibrator brightness temperature and the antenna beam pattern. Effects of antenna and receiver properties (gain, bandwidth, physical temperature and attenuation of the components between the antenna mouth and the radiometer output) are included in  $G$ .

With one important exception (Stankevich et al. 1970) astronomical objects have been rarely used as absolute calibrators. In fact unless the source is isolated, it completely fills the antenna beam and its brightness distribution is precisely known, the accuracies of  $T_x^{eff}$ ,  $G$  and  $T_a$  are poor. Artificial blackbodies, shaped to fit the antenna aperture, to match the antenna impedance and to fill the antenna beam, are more convenient calibrators, because their effective and brightness temperatures coincide. They have been used (Bensadoun et al. 1992) at frequencies  $\nu > 1$  GHz ( $\lambda < 30$  cm) where the radiation wavelength, the antenna aperture  $A_e = \lambda^2/\Omega_a$  ( $\Omega_a$  is the antenna solid angle), and the blackbody dimensions are reasonably small. Small dimensions make also possible to bring the radiometer in space (e.g. (Mather et al. 1994)) or at balloon altitudes (e.g. (Kogut et al. 2006)) where atmospheric and environmental effects are negligible or absent and  $T_a \simeq T_{sky}$  (see 4.3.1 and Equation (12)).

Below 1 GHz however the antenna dimensions and the wavelength are large and discourage the construction of artificial sources which fit the antenna mouth and fill the antenna beam. Moreover, at these low frequencies observations from space or at balloon altitudes are extremely difficult and calibrations are better made injecting at some point between antenna and receiver, through a multi throw switch, the noise produced by very compact line terminations (the so called *dummy loads*) properly cooled or warmed.

In this case the effective temperature of the calibrator is:

$$T_l^{eff} = \left[ T_l^0 e^{-\tau_c} + \int_0^L T_c^0(x) e^{-\tau(x)} \left( \frac{d\tau}{dx} \right) dx \right] (1 - r^2) + r^2 T_{RX}^{eff} \quad (7)$$

where  $T_l^0$  and  $T_c^0(x)$  are the physical temperatures of the load and the transmission line *connecting* the load to the switch,  $x$  is a coordinate running on the line,  $\frac{d\tau}{dx}$  is the specific attenuation (neper per unit length) of the line,  $e^{-\tau_c}$  is the transmission of the line,  $r^2$  the power reflection coefficient of the load seen through the line and  $T_{RX}^{eff}$  is the noise temperature radiated by the receiver (see 3.4).

Usually the accuracy of  $G$  is good but  $T_a$ , being measured at the switch positions, must be corrected (see for instance Equation (11)) for the transmission  $e^{-\tau_c}$  and *thermal noise*

$$T_{noise} = \int_0^{\tau_c} T_0(x) e^{-\tau(x)} d\tau = \bar{T}_0 (1 - e^{-\tau_c}) \quad (8)$$

of the lossy components (LC) at temperature  $T_0$  distributed along the line between the switch and the antenna mouth. To limit the statistical and systematic uncertainties on  $T_{noise}$  the

temperature of these components must be low and stable. In fact Equation 8 gives:

$$(\delta T_{noise})^2 \simeq (T_o \delta \tau_{lc})^2 + (\tau_{lc} \delta T_0)^2 \quad (\tau_{lc} \ll 1) \quad (9)$$

e.g.  $0.3 \leq \delta T_{noise} \leq 3$  K if  $T_0 \simeq 300K$  and  $10^{-3} \leq \tau_{lc} \leq 10^{-2}$ . For the above reasons the values of  $T_{sky}$  measured at frequencies close and below 1 GHz have been so far less accurate than the values measured at higher frequencies.

Reviews in literature (see for instance (Sironi et al. 1999), (Zannoni et al. 1999), (Salvaterra & Burigana 2002) and Table 2) show that below 10 GHz the accuracy of  $T_{sky}$  rapidly decreases with frequency and it is very poor below 1 GHz. Moreover between 1 and 0.5 GHz the large dispersion of the error bars assigned by different observers to their results suggest that sometimes in the past not all the systematic effects were recognized. The frequency dependence of the accuracy of  $T_{sky}$  is especially evident in coordinated experiments like the multifrequency observations made by the White Mt. collaboration (Smoot et al. 1985), the South Pole collaboration (Bersanelli et al. 1993) and by Arcade (Kogut et al. 2004). These experiments cover the frequency interval 2 – 100 GHz and approach the frequency region close to 1 GHz where neither  $T_{CMB}$  nor  $T_{gal}$  are dominant and the models of  $T_{gal}$  and  $T_{uers}$  are insufficient to extract with the desired accuracy the cosmological signal. Additional observations at even lower frequencies were subsequently made at 1.4 GHz, 0.82 and 0.61 GHz ((Bensadoun et al. 1993), (Sironi et al. 1990) and (Sironi et al. 1991)). Unfortunately those last observations used different systems and were not coordinated among them nor with previous observations at the same or at higher frequencies. TRIS has been planned to carry on coordinated observations between 0.6 and 2.5 GHz with the aim of improving the accuracy of the existing data.

### 3. TRIS

TRIS is a set of three absolute radiometers which operate in total power configuration. All the radiometers have the same antenna beam, similar receivers and include an External Calibrator unit and an Internal Calibrator unit (see Figure 1).

The frequencies of operation (0.6 GHz ( $\lambda= 50$  cm), 0.82 GHz ( $\lambda= 36$  cm) and 2.5 GHz ( $\lambda= 12$  cm)) were chosen because they span a frequency region where the ratio ( $T_{gal}/T_{CMB}$ ) is  $> 1$  at low frequencies and  $< 1$  at high frequencies and because were used in the past for similar observations.

### 3.1. Antennas

To have the same beam the three antennas are geometrically scaled (i.e. their linear dimensions are the same in wavelength units). We chose pyramidal rectangular horns with corrugated (thin corrugations) E-plane walls and a corrugated E-plane corona at the mouth (see Table 3) because they have measurable and/or calculable electromagnetic properties. These antennas have a beam solid angle  $\Omega_a$  wide enough to dilute the contribution of isolated sources well below the signal produced by the diffuse radiation but capable to keep track of the main features of the radiation spatial distribution. Side and back lobes are low ( $\leq -30$  dB, Figure 2) to minimize spill-over from the ground and interferences. The e.m. signal is extracted from the antenna through a tunable (five tuning stubs) coaxial - waveguide transition. A prototype of the complete antenna at 8.2 GHz was built and tested in anechoic chamber. Then the 2.5 GHz was made scaling the 8.2 GHz unit and optimizing the waveguide - coaxial transition. The 0.6 and 0.82 GHz horns were then scaled from it. Horn walls, corrugations, corona, waveguide sections and waveguide-coax transition are made of anticorodal riveted plates. These parts are fastened with screws for easy disassembling and transportation (before going to Campo Imperatore the 0.82 and 2.5 GHz horns were used at the Amundsen Scott base at South Pole). Aluminum tape on all the joints provides optimum electrical contacts among the various parts and makes them insensitive to variable weather condition and oxidation.

The 0.6, 0.82 and 2.5 GHz units were too large for the available anechoic chambers. The horn beam was therefore measured on the 8.2 GHz prototype in anechoic chamber and at a test range, putting special care on side and back lobes. Results, presented in Figure 2, give a beam solid angle of  $18^\circ(E) \times 23^\circ(H)$  (HPBW). Tests on the 0.6, 0.82 and 2.5 GHz units, made looking at the transit of the sun, confirmed it.

The transmission  $e^{-\tau}$  of the components which bring the signals from the antenna throat to the receiver were measured at 0.6, 0.82 and 2.5 GHz with a Vector Network Analyzer (Agilent 8510C) in laboratory. The attenuations of the horn between mouth and throat was calculated. Results are shown in Table 4.

At Campo Imperatore the three antennas were on an almost East West row, on stands which allow to steer the beam along the E-plane. This plane is tilted  $7^\circ$  from the N-S plane in direction N $\rightarrow$ NE and S $\rightarrow$ SW. This plane crosses the southern profile of the surrounding mountains at azimuth  $187^\circ$  where there is a brief levelling (see Figure 3).

### 3.2. External Calibrator

A SPTT (Single Pole Triple Throw) switch is used to link the receiver to the antenna, the cold calibrator or the warm calibrator. The switch is a source of thermal noise. The maximum accuracy one can reach in evaluating it, is set by the repeatability of the switch attenuation and by the stability of its temperature (see eqs.(8) and (9)). To minimize this noise and its fluctuations, the switch is cooled at temperatures comparable to the sky temperature and is stabilized putting it in a bath of liquid helium. Because no commercially available units satisfied our needs, we studied and built a cryogenic, purely passive, manually driven, resonant coaxial SPTT switch based on  $\lambda/4$  lines (Zannoni et al. 1999). With  $\tau \leq 0.01dB$  and  $\delta\tau \leq 2.3 \times 10^{-3}$  it gives  $\delta T_{noise,switch} \leq 10$  mK when cooled at 3.967 K, the boiling temperature of liquid helium at Campo Imperatore (2000 m a.s.l.). When cooled the switch can be driven through fiber glass rods which come out from the dewar housing it.

#### 3.2.1. Cryogenic Waveguide

To minimize their thermal noise all the lossy components distributed between the horn throat and the receiver input are cooled. The cryogenic SPTT switch, the waveguide-coaxial transition and two 50  $\Omega$  dummy loads are mounted at the bottom of a dewar (see Figure 4) where they are always plunged in liquid helium (LHe). The third load is at the top of the dewar, at a stable temperature close to the external ambient temperature. A special stainless steel waveguide section brings the electromagnetic signal from the waveguide transition to the dewar top where it can be attached to the horn throat.

The stainless steel guide section is a thermal insulator. A window made of a polyethylene sheet in the collar at the top of the stainless steel section and two fluorglass (a special fabric transparent to radio and microwaves, opaque to IR) sheets in the stainless steel waveguide limit the input of thermal radiation. Holes in the fluorglass windows allow a uniform distribution of the cold helium vapors inside the waveguide.

A cable which goes through the flange at the dewar mouth links one of the two cold dummy loads to the circulator third port in the Internal Calibration Unit (see Figure 1). A second cable links the switch output to the receiver input. The three inputs of the switch go to: 1) the antenna coaxial input through a very short piece of cable at LHe temperature; 2) the second cold dummy load (the *cold source*); 3) the load at the top of the dewar (the *warm load*) through a long cable. Sensors monitor the level of the liquid helium and the temperatures of switch, cold and warm loads, waveguide walls and cables inside and outside the dewar.

A 250 l dewar can house the 0.6 or the 0.82 GHz system. It is sufficient to carry on observations for more than 48 hours without refilling. The 2.5 GHz system is in a 100 l dewar. Once filled with helium it allows continuous observation for about 90 hours.

The effective temperatures of the cold loads are larger than 3.967 K, the boiling temperature of LHe at the observing site, because of the unavoidable e.m. mismatches which carry in a fraction of the noise temperature radiated by the receiver (see Equation 7 and Table 5). Their values however can be calculated. The high value of  $T_{cl}^{eff}$  at 2.5 GHz is a consequence of the increasing difficulties of matching resonant systems when the wavelength decreases. The complete structure of the horn and Cryogenic Waveguide is shown in Figure 4.

### 3.2.2. Warm Waveguide

A more simple calibrator based on a small dewar containing just the SPTT switch and the three dummy loads was also prepared. It requires a limited quantity of LHe. It was used for preliminary tests and for 0.82 GHz absolute measurements when the dewar of the cryogenic waveguide failed. The final accuracy one gets on  $T_{sky}$  is however worse compared to the accuracy one gets using the Cryogenic Waveguide because of the noise produced by the lossy components, including the waveguide - coaxial transition, at ambient temperature.

## 3.3. Internal Calibrator and Reflectometer

A combination of circulators, directional couplers, solid state noise source, matched dummy loads and electrically driven switches form a unit, mounted between the receiver input and the Low Noise Amplifier (see Fig.1 IntCal block). It can be used to:

- i) check the e.m. matching of the components attached at the receiver input. This is done turning on the solid state noise source and sending its signal toward the receiver input. The measured variations of the receiver outputs  $\Delta O_{inj}$  and  $\Delta O_{ref}$  when the receiver input is, respectively, short circuited or connected to the device under test, give the *power reflection coefficient*  $r^2 = \Delta O_{ref} / \Delta O_{inj}$  (*reflectometer mode*).
- ii) check the receiver gain sending the noise generator signal into the receiver (*internal calibration mode*).
- iii) set to a known level the effective temperature  $T_{RX}^{eff}$  of the noise the receiver radiates toward the antenna. This is the *effective noise temperature*  $T_N^{eff}$  of the load at the third port



of the circulator (see Equation (7) and Figure 1). When this load is cooled at liquid helium temperature (see below)  $T_{RX}^{eff}$  can be of few tens of K.

The internal calibrator and the reflectometer are used for regular checks of the radiometer performance during the observations. Cross checks are made on site with a scalar network analyzer.

### 3.4. Receivers

TRIS receivers are standard heterodyne chains with double frequency conversion, total gain of  $\sim 100$  dB, used in total power configuration (see Figure 1 and Table 5). The frequency of the Local Oscillator LO1 can be adjusted digitally (see Figure 1) so one can tune the observing channel among 256 adjacent frequencies separated by  $\Delta\nu$ , symmetrically distributed around the system nominal frequency  $\nu_o$ .  $\Delta\nu$  is 75 KHz at 0.6 and 0.82 GHz, spanning a range of 20 MHz, and 750 KHz at 2.5 GHz, over a range of 200 MHz. The integration bandwidth is 0.3 MHz at 0.60 and 0.82 GHz and 3 MHz at 2.5 GHz one.

The post detection integration time constant is 10 sec. After integration the receiver output is sampled and digitally converted every 4 sec. Each sampled value, the housekeeping data and the time signal are written in a record and stored on the hard disk of the Personal Computer which drives the local oscillator LO1. The time signals arrive from a master clock locked to radio signals regularly transmitted by I.E.N. Galileo Ferraris in Turin. The same clock drives the computer clock and guides the observational sequence. To avoid digital noise the 20-bit AD converter is integrated into the detector channel and data are transmitted via optocoupler to the data recording system.

Measurements in total power configuration can be affected by gain instabilities. To compensate for them the receiver detection channel includes zero-bias Schottky diodes and temperature stabilization of the DC section (active control with accuracy better than  $0.1^\circ C$ ). The receiver temperature is set at stable values ( $\pm 0.1^\circ C$ ) chosen between  $25^\circ C$  and  $35^\circ C$  for excursions of the external temperature from well below zero up to the preset value (usually  $+35^\circ C$ ). Gain variations can be monitored and, when necessary, recovered looking at the amplitude of the internal calibrator signal (see below). They are usually small ( $\leq 2\%$ ) except in rare occasions during observations around the local noon when clear sky and no breeze may bring the external temperature of the receiver box above the preset value. When this situation occurs data are rejected.

## 4. Observations

Between 1990 and 1993 prototypes of the three radiometers and antennas were installed at Campo Imperatore (lat. =42° 26' N, long.= 13° 33' E), a plateau 2000 m a.s.l.. The site is reasonably shielded against unwanted signals from the horizon by a circle of low elevation mountains (see Figure 3). Served by road in summer and by cable car in winter, the site is on the vertical of the underground Laboratori Nazionali del Gran Sasso (LNGS) which provided logistical support. This accommodation is a reasonable compromise between ideal places not easily accessible (like Antarctica) or isolated places with no facilities available (like White Mt. (California) or Alpe Gera (Italian Alps)) we used in the past.

Various tests were made at Campo Imperatore between 1991 and 1995. They showed that in spite of the mountain circle, interferences from horizon directions were occasionally present and forced us to observe only at the zenith. The final installation of TRIS radiometers was made between summer 1997 and summer 1998. After repeated observations dedicated to find clean frequency channels, differential measurements (drift scans) began. They continued in 1999 when tests of the cryogenic front ends were completed. Absolute measurements of the sky temperature were made in June and October 2000. Drift scans were then resumed and continued until May 2001 when antennas were removed from Campo Imperatore.

### 4.1. Modes of operation

Three modes of operation have been used with TRIS:

*Interference Search Mode.* The PC drives the Local Oscillator and tunes cyclically the receiver through the 256 frequencies distributed around the receiver nominal frequency  $\nu_o$  (10 minutes/channel). Simple statistics (mean and standard deviation) have been used to recognize channels disturbed by interferences and to choose quiet channels where observations were possible. Searches lasting at least 24 h were repeated at various epochs. At 0.6 and 0.82 GHz we found frequencies free from interferences. The best were 0.6005 and 0.8178 GHz. At 2.5 GHz no frequency completely free from interferences was found. The best one was 2.4278 GHz. These frequencies are those used for the final observations in both the following modes.

*Absolute Measurement Mode.* The antenna is aimed at the zenith. The horn throat is attached to the collar of the cryogenic front end. A couple of hour after filling (or partial refilling) with LHe, the system is in thermal equilibrium and observations are possible. Moving the switch manually the receiver input is cyclically connected to the Cold Source (receiver output  $S_{cold}$ ), the Antenna (receiver output  $S_{sky}$ ) and the Warm Source (receiver

output  $S_{warm}$ ). Each step of the cycle lasts 10 minutes during which 15 records/minute are stored on the PC hard disk. Each record contains  $S_x$ , UT time, Julian day, temperature of loads and lossy components between switch and antenna mouth, housekeeping data. The cycle of three steps is repeated few times then the switch is set on the Antenna position and observation goes on for about one hour recording  $S_{sky}$ . At regular time intervals the solid state noise source is set on and data necessary to check gain stability and power reflection coefficients  $r^2$  of the source at the receiver input are recorded.

Absolute measurements are made only at nighttime, when the observing conditions are good and the dewar full of LHe well above the top of the waveguide coaxial transition. At 0.6 GHz observations with the Cryogenic Waveguide went on regularly. At 0.82 GHz we began observation in June using the Cryogenic Front End but the dewar failed because of a leakage in the vacuum tank. We fixed it but in October, when after the 0.6 GHz run we moved at 0.82 GHz, the dewar failed again and we had no possibility to fix it again before leaving Campo Imperatore. So at 0.82 GHz we have only absolute measurements made as preliminary tests in June, using the cryogenic switch cooled with liquid helium and the completely warm antenna. This system worked very efficiently, but because all the horn components, including the waveguide-coaxial transition, were at ambient temperature, final results at 0.82 GHz are less accurate than at 0.6 GHz.

The absolute measurements at 2.5 GHz with the Cryogenic Waveguide went on regularly but were plagued by interferences.

*Drift Scan Mode.* Records with  $S_{sky}$  and the associated information are stored continuously every 4 sec while the sky transits through the antenna beam aimed at the zenith. In this mode we look at the variations of  $S_{sky}$  with Right Ascension and do not care of the signal zero level, provided it is stable. The antenna can be attached to the dewar (no matter if cold or warm) with the switch on position 2 or attached directly to the receiver via an ambient temperature coaxial-waveguide transition. Gain stability and antenna power reflection coefficient are measured automatically two times per hour. In this mode the radiometers can work unattended for weeks. Because data collected at daytime and more noticeably around noon are usually contaminated by the sun emission, to cover the entire ( $0^h - 24^h$ ) Right Ascension interval drift scans are repeated months apart.

Drift scan data were collected during the entire lifetime of TRIS. The more systematic observations were made from 1998 on. At 0.6 and 0.82 GHz they are sufficient to cover the entire 24 h circle of Right Ascension at  $\delta = +42^\circ$ . At 2.5 GHz the great majority of the observations were disturbed by interferences and no complete drift scans were obtained.

## 4.2. Data Reduction

First of all the raw data collected in Absolute or Drift Scan mode are *edited*. We reject all the records containing data obtained:

- i) at daytime (between half an hour before sunrise and half an hour after sunset);
- ii) less than six hour after the receiver was turned on;

or when

- iii) interferences were evident on the records;
- iv) the log book shows that the weather conditions were bad (rain, snow);
- v) the antenna reflection coefficients  $r^2$  monitored by the receiver internal reflectometer worsened (e.g because of water vapor condensation on the antenna components at sunrise or sunset);
- vi) the system gain or the noise level change or fluctuate by more than 5%.

The remaining data are then divided in blocks, continuous time series of homogeneous records, lasting at least 10 minutes. A block starts when the switch is set in a position (or when drift scan mode starts) and stops when the switch is moved to a new position or whenever a major interruption of the time series occurs. We call them *Absolute Sky*, *Cold*, *Warm* and *Drift Scan* or *Differential* blocks (or records, or data), depending on the observing mode and/or the switch position. Typical block lengths are 5-20 minutes for absolute data. The blocks of differential data can last hours.

Then we remove all the data collected in the first minute of a block time series (to account for the response time of the system) and continuous time series of differential data lasting less than three hours and separated from the following homogeneous block of data used for analysis by more than one hour.

Finally for each record we calculate and add to it  $(\alpha, \delta)$  of the antenna beam axis calculated from the recorded values of time and Julian day, the effective noise temperatures radiated by the receiver  $T_{RX}^{eff}$ <sup>1</sup> and the effective noise temperatures of Cold Load, Warm Load and Circulator third Port, respectively,  $T_{cold}^{eff}$ ,  $T_{warm}^{eff}$  and  $T_N^{eff}$  using (Equation (7)).

The resulting blocks are the data ready to be analyzed. They are treated in different

---

<sup>1</sup>When loads are well matched in Eq. (7) we can set  $r^2 \simeq 0$ , get the effective temperature of the circulator third port  $T_N^{eff}$  and set it equal to  $T_{RX}^{eff}$ . Then we repeat the calculation of the effective noise temperature of the circulator third port as seen at the switch and use this value as final  $T_{RX}^{eff}$

ways, depending on their type.

### 4.3. Absolute values of sky temperature

From pairs of time adjacent blocks of *cold* and *warm data* the gain  $G$  is obtained using Equation (6) and the average values of  $S_{cold}$ ,  $T_{cold}^{eff}$ ,  $S_{warm}$  and  $T_{warm}^{eff}$  on the block. Typical values are shown in Table 5.

Then from each value of  $S_{sky}$  in a *sky* block and  $G$  from the nearest pair of *cold* and *warm* data we get the instantaneous value of the signal temperature which arrives at the switch:

$$T_{a,sw} = T_{cold}^{eff} + (S_{sky} - S_{cold})G \quad (10)$$

The system linearity, i.e. the stability of  $G$  and its independence on the signal level, have been checked during all the calibration campaigns, by looking at the amplitude of the Calibration Mark (CM) when injected over very different level of signals: Cold Load (He), Sky and Warm Load. It is worth to underline that the CM provides an equivalent temperature in the same range of the maximum variation of antenna temperature measured by our experiment (about 20 K, 14 K and 1 K at 0.6, 0.82 and 2.5 GHz respectively). CM amplitude was constant within statistical fluctuations, setting a 0.4% upper limit to the deviation from system linearity.

The antenna temperature at the horn mouth is then

$$T_a(\alpha, \delta) = \frac{1}{1 - r^2} \left[ \left( \frac{T_{a,sw} - \int_0^{\tau_{tl}} T_{tl}(x) e^{-\tau_{tl}(x)} d\tau}{e^{-\tau_{tl}} e^{-\tau_h}} - \frac{\int_0^{\tau_h} T_h(x) e^{-\tau_h(x)} d\tau}{e^{-\tau_h}} \right) - r^2 T_{RX}^{eff} \right] \quad (11)$$

Here  $T_{tl}$ ,  $\tau_{tl}$ ,  $T_h$  and  $\tau_h$  are the temperatures and the optical thicknesses of the lossy components along the transmission line (*tl*) and the horn sections (*h*) between the switch and the antenna aperture.

#### 4.3.1. Sky Temperature

The sky brightness temperature is then:

$$T_{sky}(\alpha, \delta, \nu) = \left[ \frac{T_a(\alpha, \delta, \nu) - T_{RX} r^2}{1 - r^2} - T_{atm}^0 (1 - e^{-\tau_{atm}}) - T_{env} \right] / e^{-\tau_{atm}} \quad (12)$$

where  $\tau_{atm}$  and  $T_{atm}^0$  are the optical thickness and the average physical temperature of the atmosphere above the antenna,  $T_{env}$  the noise temperature of the environment which reaches

the antenna, usually through side and back lobes,  $T_{RX}^{eff}$  the temperature of the noise radiated by the radiometer and  $r^2$  the power reflection coefficient of the antenna.

At nighttime, when the Sun contamination is absent,  $T_{env} = T_{ground} + T_{inter}$  where  $T_{ground}$ , the effect of the ground thermal emission, is the convolution of  $P_n(\theta, \phi)$ , the normalized, three dimensional, beam profile (see Figure 2) and a blackbody at ambient temperature  $T_0$ , which fills the antenna beam up to  $h(\phi)$ , the Campo Imperatore horizon profile, (see Figure 3):

$$T_{ground} = T_0 \int_0^{2\pi} d\phi \int_0^{h(\phi)} P_n(\theta, \phi) \sin(\theta) d\theta \quad (13)$$

$T_{inter}$  is the noise produced by radio interferences. At 0.6 and 0.82 GHz channels free from interferences were found (0.6005 GHz and 0.8178 GHz). Here the interferences, if present, were completely buried in the system noise. At 2.5 GHz also in the best channel at 2.4278 GHz, even when no sudden changes of level were appreciable, the signal was unstable and the noise anomalously high, probably because of a blend of undesired signal from artificial sources at the horizon or below it. This contribution has been measured surrounding the antenna with ground shields which went well above the horizon visible from the antenna mouth and reflected all the side and back lobes on the sky.

For the atmospheric contributions we use values of absorption calculated for various sites, including Campo Imperatore, by (Ajello et al. 1995) from a collection of vertical profiles of the earth atmosphere collected for one year with sounding balloons launched daily at meteo stations. Results are shown in Table 6.

The above values of  $T_{sky}$ ,  $T_a$ ,  $T_{a,sw}$  are oversampled because the TRIS sampling time (4 sec) is shorter than the system time constant (10 sec). To make them statistically independent in each *sky block* data are binned in groups of at least 50 sec and averaged. The average values and standard deviations of  $T_{sky}$  in a bin are considered representative of the absolute brightness temperature of the sky at  $(\langle \alpha \rangle, \langle \delta \rangle)$  only if they come from a block close (*few tens of minutes*) to the pair of *cold* and *warm* data used to get  $G$  and  $T_{cold}^{eff}$ . This because  $G$  and  $T_{cold}^{eff}$  are helium level dependant and the level is practically constant within this period of time.

#### 4.4. Drift scans of the sky temperature

The edited time series of *drift scans* data are from observations made in separate years at different times of the year, in different conditions.

During the drift-scan mode observations, every component of the radiometers was at ambient

temperature, with the receivers always operating in a temperature controlled box. In this configuration, the data were taken continuously for months. We decided to reject daytime data. Moreover, bad weather conditions and interferences didn't allow us to exploit all the night-time data collected, therefore it took more than one year to cover all the  $\delta = +42^\circ$  sky circle since the last TRIS configuration (antennas in vertical position, receivers in total power configuration) was established. We combined data taken at different times by virtue of the internal and stable noise source (CM), whose signal was periodically (two times every  $48^m$ ) injected towards the antenna port of the circulator in order to check the SWR (*reflectometer mode*) and, after that, towards the receiver port as a calibration mark<sup>2</sup>. In this way, we could associate a value of the CM to every set of observations. The different sets were then normalized to the reference CM measured during absolute calibrations. We have been able to find time sequences of good data (good weather conditions, no radio interferences) lasting more than 48 hours. This allowed to compare nighttime data separated up to two sidereal days and correct for linear drifts of the signal (if present). The nighttime data, corrected for drift and renormalized by means of the CM, have been seamed at common RA. Integration of all the nighttime profiles acquired during the life of the experiment gives the final profile. Its scale, in ADU and arbitrary zero level, was then converted to temperature scale and zero adjusted fitting the profile to the absolute values of sky temperature measured during calibration sessions. The reconstruction of the full sky profiles at 0.6 GHz and 0.82 GHz deserves some other comments. The calibration mark signals have a very small dispersion, witnessing the stability of the system all along the observational campaign. In fact the sample collected during several months at 0.6 GHz had a mean value around 24000 ADU, while the mean standard deviation set around 20 ADU. The corresponding quantities at 0.82 GHz were respectively 19500 ADU and 30 ADU.

The error budget on the two definitive profiles at 0.6 and 0.82 GHz are then dominated by the uncertainties due to the correction for the linear drifts and offsets and by the uncertainty in the determination of the temperature scale. In particular, along the galactic halo region ( $8^h \lesssim \alpha \lesssim 16^h$ ), which has been observed redundantly, the definitive uncertainty upon temperature variations are in the range 5 – 10 mK both at 0.6 GHz and 0.82 GHz, depending on the sky position (this uncertainty rises to 30 – 40 mK near the galactic plane, where we have collected a smaller number of drift scans).

By this procedure we recover the full dynamic of the celestial signal up to the antenna mouth and above the earth atmosphere. Results are shown in Figure 5. This procedure worked successfully at 0.6 and 0.82 GHz. At 2.5 GHz the construction of drift scan profile

---

<sup>2</sup>The calibration mark is the value above the noise floor of the signal injected by the noise generator, expressed in analog-to-digital units (ADU). The gain is properly the conversion factor K/ADU.

was hampered by the interference level which frequently covered the sky signal. The few observing hours when interferences were small are so sparse that we couldn't build a clean drift scan profile.

## 5. Discussion

The absolute values of  $T_{sky}(\alpha, \delta)$  measured by TRIS at 0.6005 GHz, 0.8178 GHz and 2.4278 GHz, at selected points of constant declination  $+42^\circ$  are listed in Tables 7, 8 and 9. The same data are plotted in Figure 5 together with the drift scans (0.6 GHz and 0.82 GHz are reported in Tables 10 and 11). Having no reliable drift scan at 2.5 GHz, we built a profile only of the galactic component starting from the Stockert (Reich & Reich 1986) survey at 1.420 GHz. This map has been convoluted to the beam of the TRIS antennas in order to get the synthetic drift scan at  $\delta = +42^\circ$ . Then we compared this scan with the pure galactic signal we evaluated at 0.6 and 0.82 GHz (see Papers II and III). Using these measurements we evaluated the galactic emission first at 1.420 GHz and then extrapolated it at 2.5 GHz, using the local spectral index evaluated between 0.6 and 0.82 GHz. We used the local spectral index because it is a well defined quantity throughout all the sky provided that absolute galactic emissions measurements are available, which is our case. We used the map at 1.42 GHz because it is the closest one, public domain, at the frequency 2.5 GHz. In Figure 5 at 2.5 GHz, for uniformity with the measured sky profiles plotted at 0.6 and 0.82 GHz, we added over the TRIS absolute sky temperatures a profile (dashed line) obtained summing to the galactic component calculated as described above, the Unresolved Extragalactic Radio Sources contribution (Gervasi et al. 2008b) and Cosmic Microwave Background (Gervasi et al. 2008a).

The systematic uncertainties are computed propagating through Equation (11) and (12) the uncertainties on the measured values of attenuation and temperature of the lossy components between the switch and the antenna mouth. The losses are very small. In some cases they are so small that measurements give only upper limits (see Table 4) and the range of fluctuation of the true losses is unknown but reasonably smaller and well inside the upper limit, set by the accuracy of the instrumentation used to carry on the measurements. The final uncertainties on the sky temperature obtained propagating these errors are therefore considered as systematic. At 0.6 GHz the great majority of the components is cold ( $\sim 4$  K) and the final systematic uncertainty is small (66 mK). At 2.5 GHz the systematic uncertainty is worse because of the quality of the e.m. matching of the SPTT switch and the presence of an additional section of warm waveguide between the dewar flange and the antenna throat. This correction contributes to the systematics for 284 mK. At 0.82 GHz the systematic



uncertainty is very large, 660 mK, essentially because all the components above the switch were warm and at high temperature (see Equation 9). Such a large value, however, does not take into account constraints set by unphysical situations (e.g. negative values of the temperature of the diffuse radiation components and values of the galactic spectral index not supported by models of galactic emission). When astrophysical assumptions are made on these values (for a complete discussion see Paper III) the systematic uncertainty at 0.82 GHz is reduced to  $(^{+430}_{-300})$  mK.

The above results hold if the sky radiation is unpolarized. We know however that the galactic component of  $T_{sky}$  is partially polarized and that polarization is linear. Since antennas are polarized, our measured values of the sky temperature are better written as

$$T_{sky}(\alpha, \delta, \nu) = T_{CMB}(\nu) + T_{uers}(\nu) + T_{gal}^{unpol}(\alpha, \delta, \nu) + T_{gal}^{pol}(\alpha, \delta, \nu) \cos^2[\theta(\alpha, \delta, \nu) - \theta_0] \quad (14)$$

where  $T_{gal}^{unpol}$  and  $T_{gal}^{pol}$  are respectively the unpolarized and polarized components of the galactic signal, and  $(\theta - \theta_0)$  is the angle between the polarization vector of the radiation and the polarization vector of the antenna.

The true sky temperature is therefore

$$T_{sky}^{true}(\alpha, \delta, \nu) = T_{sky}^{unpol}(\alpha, \delta, \nu) + T_{sky}^{pol}(\alpha, \delta, \nu) = T_{sky}(\alpha, \delta, \nu) + \Delta T^{pol}(\alpha, \delta, \nu) \quad (15)$$

where

$$\Delta T^{pol}(\alpha, \delta, \nu) = T_{gal}^{pol}(\alpha, \delta, \nu) \sin^2[\theta(\alpha, \delta, \nu) - \theta_0] \quad (16)$$

is the signal lost. Were circular polarization present, an additional term should be added to Equation (15).

The information today available on the polarization degree and direction of the diffuse radiation is limited. We do not expect circular polarization. Linear polarization on the contrary must be expected but the information available is poor. Below 1 GHz there are only data obtained thirty years ago by (Brouw & Spoelstra 1976). The assessment of the overall sky temperature has been obtained correcting our absolute measurements for the fraction of the linearly polarized signal. In order to do this we used the Brouw and Spoelstra maps of the Stokes Parameters Q&U in the resampled version prepared by E.Carretti in the framework of the SPOrt program (Cortiglioni et al. 2004). Carretti maps having  $7^\circ$  resolution, were further convolved with the beam of our experiment. Then, considering the relative orientation of the polarization plane (E-plane) of our antennas and the polarization of the celestial signal, we projected the polarized vector into Copolar (collected by our antennas) and Crosspolar components (rejected by our antennas). We conclude that, at

TRIS angular resolution, the maximum contribution of the polarized signal to the overall one, around 2% at 0.6 GHz and 3% at 0.82 GHz, comes mostly from regions far from the galactic disk. This result is in agreement with Platania et al. (1998) who gives a maximum contribution of  $\sim 5\%$  at 0.408 GHz with a  $18^\circ$  beam in a sky region very close to the one scanned by TRIS. A detailed discussion can be found in Paper III. Between 1 and 3 GHz more recent and accurate data are available (see for instance (Duncan et al. 1999), (Wolleben et al. 2006) and references therein), but with few exception they do not fill all the areas covered by TRIS scans. Full sky models of the galactic synchrotron intensity and linear polarization prepared for feasibility studies of forthcoming space experiments (e.g. (Giardino et al. 2002), (Bernardi et al. 2003)) are available. However we preferred to evaluate the polarized component starting from real data acquired at frequencies close to the TRIS ones. Considering that at 2.5 GHz with the TRIS angular resolution ( $T_{gal}/T_{sky} \simeq (T_{gal}/T_{CMB}) \leq 0.1$  and  $T_{gal}^{pol} \leq T_{gal}$ , we can assume also at 2.5 GHz ( $\Delta T^{pol}/T_{sky}^{true} < 0.02$ ).

In conclusion, neglecting the polarization effects is equivalent to introduce an additional systematic uncertainty on the true values of the sky temperature of less than 3% (see Table 12).

Table 13 gives a list of measurements of  $T_{sky}$  present in literature at frequencies comparable to the frequencies used by TRIS, the value of the derived  $T_{CMB}$  and the associated uncertainties for  $T_{sky}$  and  $T_{CMB}$ . All the values of  $T_{sky}$  have been obtained as intermediate steps of experiments aimed at getting the CMB temperature, so papers usually focus the reader attention on the accuracy  $\sigma_{CMB}$  of  $T_{CMB}$ . The accuracy  $\sigma_{sky}$  of  $T_{sky}$  should be better ( $\sigma_{sky} < \sigma_{CMB}$ ) but extracting it from papers it is not always possible. When no detailed information is available in literature we assume  $\sigma_{sky} \leq \sigma_{CMB}$ . It appears that at 0.6 and 0.82 GHz the TRIS absolute values of the sky temperature are the best today available. At 2.5 GHz TRIS results are less accurate than data obtained in the past by us with the White Mt. and the South Pole collaborations. Nevertheless we report also the TRIS results at 2.5 GHz because they came exactly from the same direction and have been obtained with the same angular resolution of our observation at lower frequencies.

TRIS data can be used to

- i) disentangle the components of the diffuse radiation,
- ii) extract the cosmological and astrophysical information carried by these components,
- iii) improve zero level and scale of temperature of the full sky maps of the diffuse radiation at decimetric wavelength in literature (see Tables 1 and 2).

These types of analysis are intricate and require different approaches, depending on

the final aim: astrophysical or cosmological conclusion. They are done in separate Papers II (Gervasi et al. 2008a), III (Tartari et al. 2008) and (Gervasi et al. 2008b) which accompany present Paper I. Here (Table 14) we present a summary of the results discussed in the cited papers. We have reduced the error bars on  $T_{CMB}$  of a factor 9 at  $\nu = 0.6$  GHz and of a factor 7 at  $\nu = 0.82$  GHz. These results have been possible because of the improvements in the absolute calibration system and in the foregrounds separation technique. At 2.5 GHz TRIS did not improve the previous measurements, but is in agreement with them.

**Acknowledgements:** The TRIS activity has been supported by MIUR (Italian Ministry of University and Research), CNR (Italian National Council of Research) and the Universities of Milano and of Milano-Bicocca. The logistic support at Campo Imperatore was provided by INFN, the Italian Institute of Nuclear Physics, and its Laboratorio Nazionale del Gran Sasso. We are indebted with E. Carretti who provided us a low resolution polarized map based on the Brouw and Spoelstra one. We are also grateful to R. Nesti for some crucial simulations of the horn attenuations. We acknowledge the contributions and comments by many peoples, among them G. Bonelli, A. Grillo, C. Cattadori, G. De Amici, E. Pagana, G. Navarra, of members of the LNGS technical staff A. Fulgenzi, G. Adinolfi, L. Masci, G. Giuliani. Frequently students who were preparing their thesis for the degree in Physics took part to TRIS activities. We acknowledge the use of the HEALPix package (Gorski et al. 2005) to evaluate the polarized galactic signal at 0.610 and 0.82 GHz.

## REFERENCES

- Ajello, C., Bonelli, G., Sironi, G., 1995, ApJS 96, 643
- Bensadoun, M., Witebsky, C., Smoot, G., de Amici, G., Kogut, A., Levin, S., 1992, RSciI 63, 4377-4389
- Bensadoun, M., Bersanelli, M., de Amici, G., Kogut, A., Levin, S. M., Limon, M., Smoot, G. F. Witebsky, C., 1993, ApJ, 409, 1
- Berkhuijsen, E.M., 1972, A&A, 5, 263
- Bernardi, G., Carretti, E., Cortiglioni, S., Sault, R.J., Kesteven, M.J., Poppi, S. 2003, ApJ, 594, L5
- Bersanelli, M., Bonelli, G., Sironi, G. et al., 1993, Antarctic Journal XXVIII, 306
- Bersanelli, M., Bensadoun, M., de Amici, G., Levin, S., Limon, M., Smoot, G. F., Vinje, W., 1994, ApJ424, 517

- Brouw, W.N. and Spoelstra, T.A.T., 1976, A&A Suppl., 26, 129
- Burigana, C. and Danese, L. and de Zotti, G., 1991, A&A, 246, 49B
- Cortiglioni, S. et al., 2004, New A, 9, 297
- Duncan, A.R., Reich, P., Reich, W., Fuerst, E., 1999, A&A, 350, 447
- Fixsen, D.J & Mather, J.C. 2002, ApJ, 581, 817
- Gervasi, M., Zannoni, M., Tartari, A., Boella, G., Sironi, G., 2008a, ApJ, *submitted*
- Gervasi, M., Tartari, A., Zannoni, M., Boella, G., Sironi, G., 2008b, ApJ, *in press*, arXiv:0803.4138v1
- Giardino, G., Banday, A.J., Gorsky, K.M., Bennet, K., Jonas, J.L., Tauber, J., 2002, A&A 387, 82
- Gorski, K. M., Hivon, E., Banday, A. J., Wandelt, B. D., Hansen, F. K., Reinecke, M., Bartelmann, M., 2005, ApJ, 622, 759
- Haslam, C. G. T., Salter, C. J., Stoffel, H. and Wilson, W. E., 1982, A&AS, 47, 1
- Howell, T.F. & Shakeshaft, J.R., 1967, Nature, 216, 7
- Jonas, J., Baart, E.E. and Nicolson, G.D., 1998, MNRAS, 297, 977
- Kogut, a., Fixsen, D.J., Levin, S., Limon, M., Lubin, P.M., Mirel, P., Seiffert, M. and Wollack, E. 2004, ApJSuppl. 154, 493
- Kogut, A., Fixsen, D., Fixsen, S., Levin, S., Limon, M., Lowe, L., Mirel, P., Seiffert, M., Singal, J., Lubin, P., Wollack, E., 2006, New A Rev., 50, 925
- Landecker, T.L. & Wielebinsky, R., 1970, Austr. J. Phys. Suppl., 16, 1
- Mather, J. C. et al, 1994, ApJ 420, 439
- Milogradov-Turin, J., 1984, MNRAS, 161, 269
- Otoshi, T.Y. & Stelzried, C.T., 1975, IEEE Trans. Instrum. Meas. 24, 174
- Pelyushenko, S.A. and Stankevich, K.S., 1969, Sov. Ast. 13, 223
- Platania, P., Bensadoun, M., Bersanelli, M., De Amici, G., Kogut, A., Levin, S., Maino, D. & Smoot, G.F., 1998, ApJ, 505, 473

- Platania, P., Burigana, C., Maino, D., Caserini, E., Bersanelli, M., Cappellini, B. and Men-  
nella A., 2003, *A&A*, 410, 847
- Reich, P. & Reich, W., 1986, *A&AS*, 63, 205
- Roger, R.S., Costain, C.H., Landecker, T.L. & Swerdlyk, C.M., 1999, *A&AS*, 137,7
- Salvaterra, R. & Burigana, C. 2002, *MNRAS*, 336, 592
- Sironi, G., Limon, M., Marcellino, G., Bonelli, G., Bersanelli, M., Conti, G., Reif, K, 1990,  
*ApJ*357, 301
- Sironi, G., Bonelli, G., Limon, M., 1991, *ApJ*, 378, 550
- Sironi, G., Boella, G., Bonelli, G., Gervasi, M., Vaccari, A. and Zannoni, M., 1999, *AIP*  
*Conf.Proc.*, 476, 149
- Smoot, G.F., De Amici, G., Friedman, S.D. et al., 1985, *ApJ*, 291, L23
- Stankevich, K.S., Wielebinski, R., Wilson, W.E., 1970, *Australian J. Phys.*, 23, 529
- Tartari, A., Zannoni, M., Gervasi, M., Boella, G., Sironi, G., 2008 *ApJ*, *submitted*
- US Standard Atmosphere. 1976, US GPO, 1976 O-599-256
- Wolleben, M., Landecker, T. L., Reich, W., Wielebinski, R., 2006, *A&A*, 448, 411
- Zannoni, M., Boella, G., Bonelli, G., Cavaliere, F., Gervasi, M., Lagostina, A., Passerini A.,  
Sironi, G. and Vaccari, A., 1999, *AIP Cof. Proc.*, 476, 165

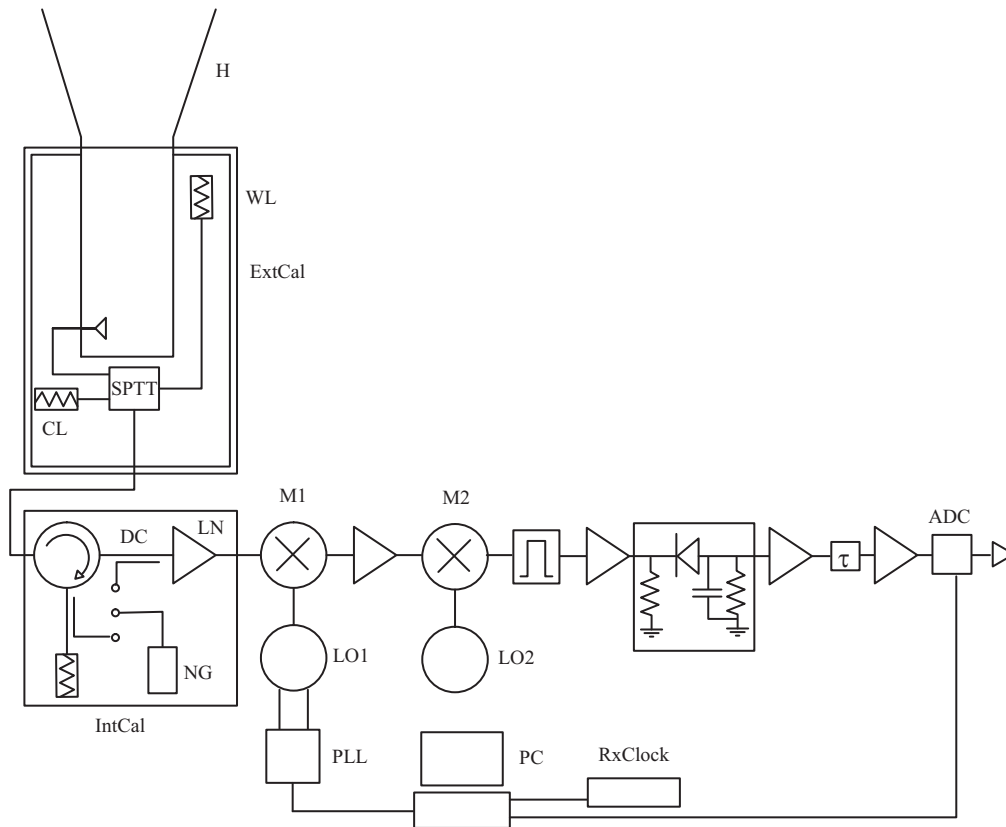


Fig. 1.— Block diagram of TRIS Radiometers H = corrugated Horn, LN = Low Noise Amplifier, LO1, LO2 = Local Oscillators, M1, M2 = mixers, PLL = Phase Locked Loop,  $\tau$  = system time constant, ADC = analog to digital converter, PC = Personal Computer, RxClock = Radio Clock, ExtCal = External Calibrator, (WL = *warm Load*, CL = *Cold Load*, SPTT = *switch*), IntCal = Internal calibrator (C = *Circulator*, DC = *Directional Coupler*, NG = *Noise Generator*)

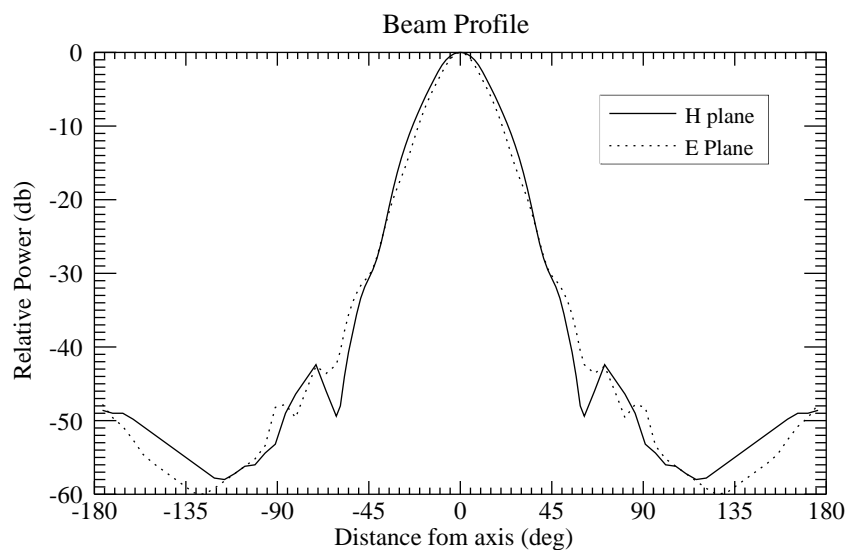


Fig. 2.— Beam of TRIS antennas measured on a geometrically scaled model at 8.2 GHz (continuous line: H-plane, dotted line: E-plane)

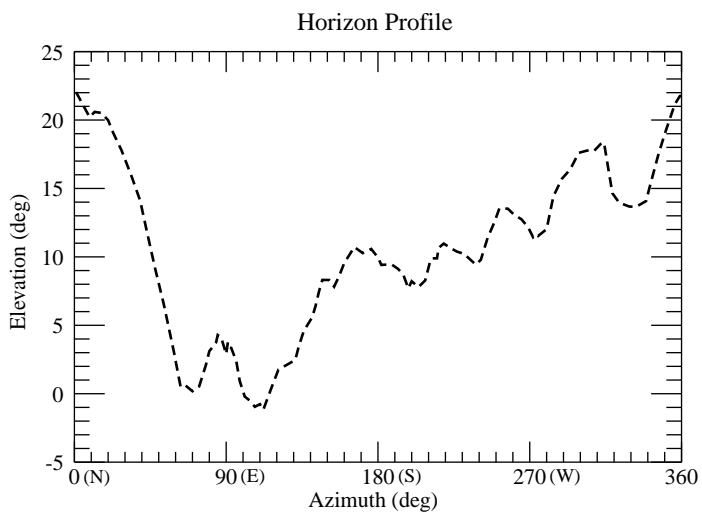


Fig. 3.— Horizon profile at Campo Imperatore

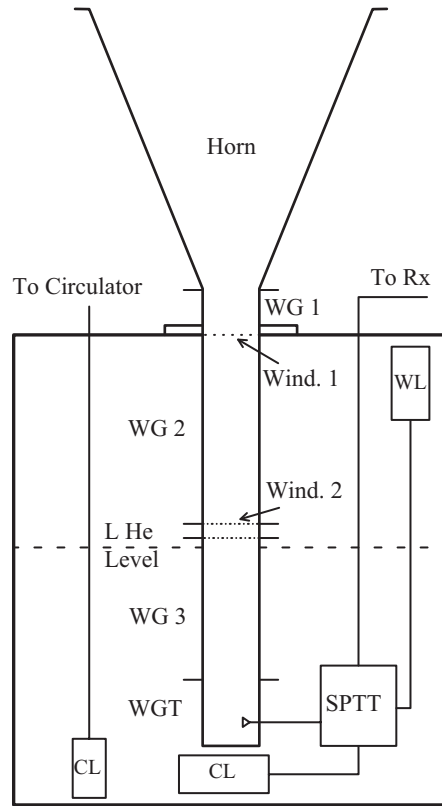


Fig. 4.— A schematic view of the Cryogenic External Calibrator (WG 1 = anticorodal waveguide section, WG 2, WG 3 = stainless steel waveguide sections, Wind. 1 = polyethylene window, Wind. 2 = fluorglass windows, WGT = brass coax-waveguide transition, SPTT = Single Pole Triple Throw switch, WL = warm dummy load, CL = cold dummy load; see also Table 4 and text)



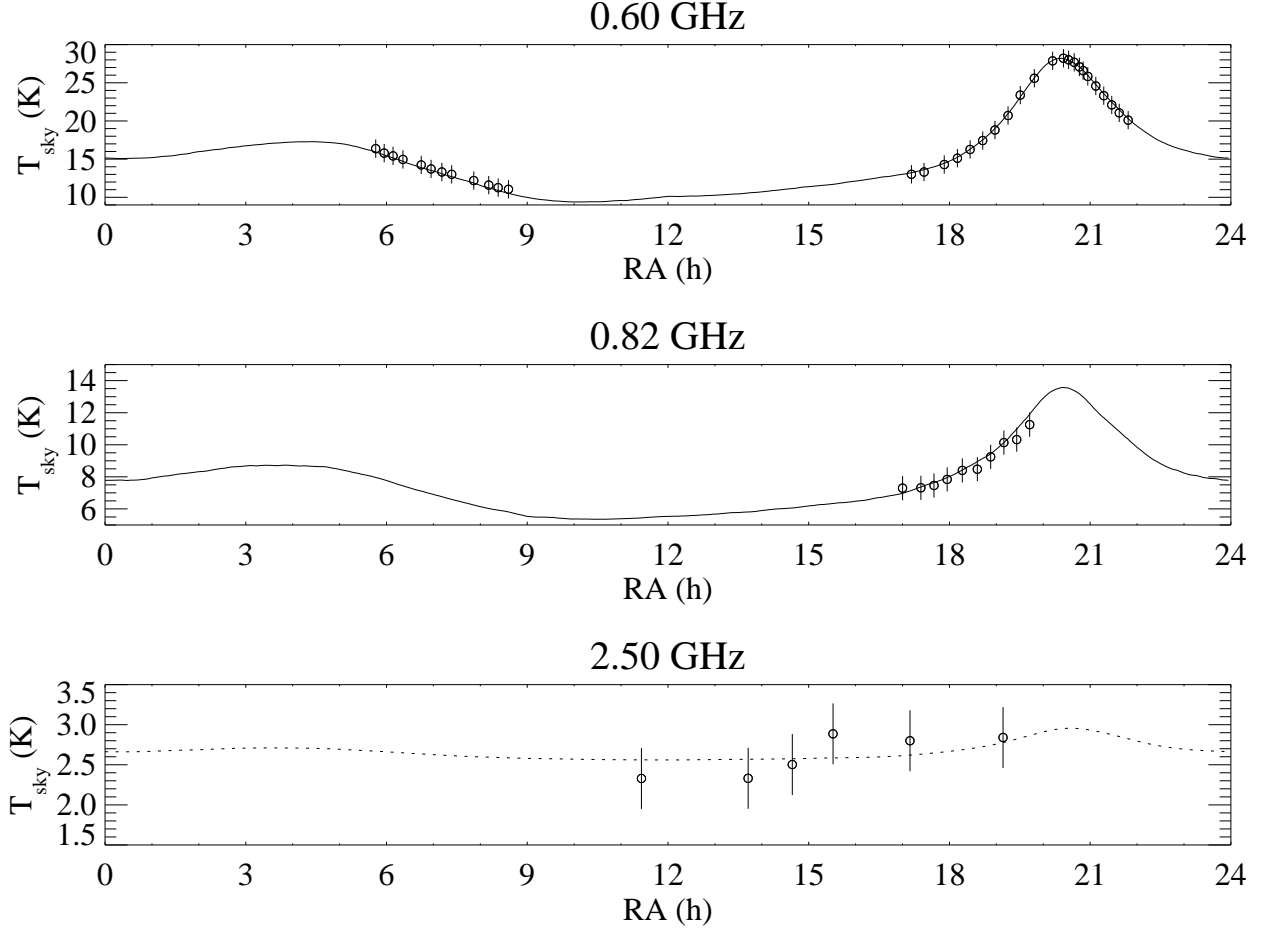


Fig. 5.— Absolute values and differential profiles of  $T_{\text{sky}}$  measured by TRIS at  $\delta = +42^\circ$ , ( $0 \leq \alpha \leq 24$ ). Uncertainties ( $3\sigma$  statistic + systematic) associated to the absolute values are indicated: to make them visible at 0.60 GHz the error bars have been enlarged by a factor 10. The zero level of the differential profiles has been adjusted to fit the distribution versus  $\alpha$  of the absolute values. At 2.50 GHz the plotted sky profile (dashed line) doesn't come from TRIS data but it has been obtained rescaling the sky profile extracted from the Stockert (Reich & Reich 1986) survey at 1.4 GHz. See Paper III for details.

Table 1. Extended maps of the diffuse radiation

$\nu$ (GHz)	$\delta T_{zero}$ (K)	$\delta T$	Angular Res.	Sky Coverage	Reference
0.022	$\simeq 10^3$	n.a.	$1.1^\circ \times 1.7^\circ$	North	1
0.038	300	5%	$7.5^\circ$	North	2
0.151	40	$\simeq 10\%$	$5^\circ$	full	3
0.408	3	$\simeq 10\%$	$0.85^\circ$	full	4
0.820	0.6	$\simeq 10\%$	$1.2^\circ$	North	5
1.420	0.5	$\simeq 10\%$	$0.6^\circ$	North	6
2.326	0.08	$\leq 5\%$	$0.33^\circ$	South	7

References. — (1) Roger et al. 1999; (2) Milogradov-Turin 1984; (3) Landecker & Wielebinsky 1970; (4) Haslam et al. 1982; (5) Berkhuijsen 1972; (6) Reich & Reich 1986; (7) Jonas et al. 1998

Table 2. Typical accuracy of measured values of  $T_{sky}$  in literature

$\nu_0$ (GHz)	$\sigma(mK)$
100 – 60	1 – 10
60 – 10	10 – 50
10 – 1	10 – 500
1 – 0.5	500 – 1500

Table 3. TRIS antennas

$\nu_0$ (GHz)	0.60	0.82	2.5
Horn Aperture	$3.7\lambda \times 4.9\lambda$	$3.7\lambda \times 4.9\lambda$	$3.7\lambda \times 4.9\lambda$
Flare Angle E Plane	$19^\circ$	$19^\circ$	$19^\circ$
Flare Angle H Plane	$23^\circ$	$23^\circ$	$23^\circ$
Phase difference $\delta_E$	$0.07\lambda$	$0.07\lambda$	$0.07\lambda$
Phase difference $\delta_H$	$0.10\lambda$	$0.10\lambda$	$0.10\lambda$
HPBW	$18^\circ(E) \times 23^\circ(H)$	$18^\circ(E) \times 23^\circ(H)$	$18^\circ(E) \times 23^\circ(H)$
Mouth Dimensions (m)	$1.85 \times 2.41$	$1.35 \times 1.79$	$0.44 \times 0.59$
Horn length (m)	2.50	1.83	0.60
Back Lobes (dB)	$< -40$	$< -40$	$< -40$

Table 4. Transmission  $e^{-\tau}$  of the TRIS front end components

component <sup>†</sup>	$\nu = 0.6$ GHz	$\nu = 0.82$ GHz	$\nu = 2.5$ GHz
WG Cable (cold)	$0.957 \pm 0.001$	$0.9698 \pm 0.0004$	$0.969 \pm 0.006$
WG Cable (warm)	...	$0.9600 \pm 0.0001$	...
WG Transition	$0.988 \pm 0.002$	$0.986 \pm 0.004$	$0.984 \pm 0.004$
WG3-1	$0.9981 \pm 0.0003$	$0.9966 \pm 0.0002$	$0.997 \pm 0.002$
wind-1	$> 0.99999$	$> 0.99999$	$> 0.99998$
WG3-2	$0.9983 \pm 0.0003$	$0.9965 \pm 0.0002$	$0.998 \pm 0.001$
wind-2	$> 0.99998$	$> 0.99998$	$> 0.99998$
WG2	$0.9989 \pm 0.0002$	$0.9997 \pm 0.0002$	$0.9995 \pm 0.0003$
WG1	$0.9983 \pm 0.0001$	$0.9991 \pm 0.0001$	$0.9985 \pm 0.0001$
WG ex	...	...	$0.9978 \pm 0.0002$
Horn	$0.9920 \pm 0.0001$	$0.9872 \pm 0.0001$	$0.9972 \pm 0.0001$

<sup>†</sup>See text and Figure 4

Table 5. TRIS receiver

$\nu_0$ (GHz)	0.60	0.82	2.5
Tunability frequency range (MHz)	20	20	200
Number of selectable frequencies	256	256	256
Integration bandwidth (MHz)	0.3	0.3	3.0
Sampling time (s)	4	4	4
Noise Temperature (K)	120	120	100
$T_{RX}^{eff}$ (K) <sup>†</sup>	84.5	67.3	72.6
$T_{cold}^{eff}$ (K) <sup>†</sup>	4.1	4.3	7.1
$T_{warm}^{eff}$ (K) <sup>†</sup>	231.4	247.2	247.1
Gain ( $10^{-4}$ K/div)	$8.498 \pm 0.004$	$7.130 \pm 0.001$	$7.234 \pm 0.001$

<sup>†</sup>Typical values (helium level dependent)

Table 6. Atmospheric and environment contributions

$\nu_0$	0.60 GHz	0.82 GHz	2.5 GHz
$T_{atm}$ (K)	$1.088 \pm 0.023$	$1.221 \pm 0.016$	$1.570 \pm 0.025$
$e^{-\tau_{atm}}$	$0.995 \pm 0.001$	$0.995 \pm 0.001$	$0.993 \pm 0.001$
$T_{ground}$ (K)	$0.07^{+0.06}_{-0.03}$	$0.07^{+0.06}_{-0.03}$	$0.07^{+0.06}_{-0.03}$
$T_{interf}$ (K)	$< 0.01$	$< 0.01$	$9.82 \pm 0.26$

Table 7. Absolute values of  $T_{sky}$  at  $\nu = 0.60$  GHz,  $\delta = +42^\circ$

$\alpha(h, m, s)$	$T_{sky}$ (K) <sup>†</sup>	$\alpha(h, m, s)$	$T_{sky}$ (K) <sup>†</sup>	$\alpha(h, m, s)$	$T_{sky}$ (K) <sup>†</sup>
05 46 00	16.372	17 11 18	13.016	20 32 35	28.007
05 57 02	15.788	17 27 31	13.315	20 39 18	27.678
06 08 26	15.423	17 53 37	14.292	20 45 59	27.084
06 20 46	14.962	18 10 12	15.123	20 50 46	26.592
06 44 22	14.241	18 26 23	16.267	20 57 11	25.839
06 57 14	13.717	18 42 33	17.437	21 07 13	24.582
07 10 34	13.319	18 58 24	18.813	21 17 17	23.312
07 23 18	13.010	19 14 56	20.715	21 27 18	22.100
07 51 39	12.193	19 30 39	23.386	21 37 20	21.061
08 10 34	11.602	19 48 22	25.593	21 48 40	20.107
08 22 56	11.264	20 12 02	27.869		
08 36 02	11.050	20 25 52	28.211		

<sup>†</sup>For error bars see Table 12.



Table 8. Absolute values of  $T_{sky}$  at  $\nu = 0.82$  GHz,  $\delta = +42^\circ$

$\alpha(h, m, s)$	$T_{sky}$ (K) <sup>†</sup>	$\alpha(h, m, s)$	$T_{sky}$ (K) <sup>†</sup>	$\alpha(h, m, s)$	$T_{sky}$ (K) <sup>†</sup>
17 00 04	7.297	18 16 29	8.401	19 26 04	10.322
17 23 29	7.319	18 35 40	8.476	19 42 39	11.256
17 40 15	7.463	18 52 43	9.249		
17 57 06	7.840	19 09 38	10.137		

<sup>†</sup>For error bars see Table 12

Table 9. Absolute values of  $T_{sky}$  at  $\nu = 2.5$  GHz,  $\delta = +42^\circ$

$\alpha(h, m, s)$	$T_{sky}$ (K) <sup>†</sup>	$\alpha(h, m, s)$	$T_{sky}$ (K) <sup>†</sup>	$\alpha(h, m, s)$	$T_{sky}$ (K) <sup>†</sup>
11 26 04	2.329	14 39 01	2.503	17 09 34	2.800
13 42 32	2.331	15 31 06	2.886	19 08 35	2.840

<sup>†</sup>For error bars see Table 12

Table 10. Sampled values of  $T_{sky}$  profile at  $\nu = 0.60$  GHz,  $\delta = +42^\circ$

$\alpha(h, m, s)$	$T_{sky}$ (K) <sup>†</sup>	$\alpha(h, m, s)$	$T_{sky}$ (K) <sup>†</sup>	$\alpha(h, m, s)$	$T_{sky}$ (K) <sup>†</sup>
00 00 00	15.145	08 00 00	11.552	16 00 00	12.117
00 30 00	15.099	08 30 00	10.683	16 30 00	12.585
01 00 00	15.204	09 00 00	9.996	17 00 00	13.023
01 30 00	15.494	09 30 00	9.576	17 30 00	13.703
02 00 00	15.986	10 00 00	9.390	18 00 00	14.747
02 30 00	16.343	10 30 00	9.412	18 30 00	16.543
03 00 00	16.745	11 00 00	9.572	19 00 00	19.201
03 30 00	17.046	11 30 00	9.801	19 30 00	23.044
04 00 00	17.242	12 00 00	10.124	20 00 00	27.015
04 30 00	17.275	12 30 00	10.168	20 30 00	28.048
05 00 00	17.050	13 00 00	10.273	21 00 00	25.628
05 30 00	16.395	13 30 00	10.442	21 30 00	22.210
06 00 00	15.443	14 00 00	10.719	22 00 00	19.323
06 30 00	14.368	14 30 00	11.058	22 30 00	17.342
07 00 00	13.438	15 00 00	11.397	23 00 00	16.204
07 30 00	12.506	15 30 00	11.682	23 30 00	15.474

<sup>†</sup>For error bars see Table 12

Table 11. Sampled values of  $T_{sky}$  profile at  $\nu = 0.82$  GHz,  $\delta = +42^\circ$

$\alpha(h, m, s)$	$T_{sky}$ (K) <sup>†</sup>	$\alpha(h, m, s)$	$T_{sky}$ (K) <sup>†</sup>	$\alpha(h, m, s)$	$T_{sky}$ (K) <sup>†</sup>
00 00 00	7.781	08 00 00	6.145	16 00 00	6.481
00 30 00	7.781	08 30 00	5.869	16 30 00	6.707
01 00 00	7.935	09 00 00	5.537	17 00 00	6.969
01 30 00	8.143	09 30 00	5.471	17 30 00	7.486
02 00 00	8.322	10 00 00	5.371	18 00 00	8.026
02 30 00	8.529	10 30 00	5.357	18 30 00	8.783
03 00 00	8.678	11 00 00	5.387	19 00 00	9.724
03 30 00	8.718	11 30 00	5.456	19 30 00	11.198
04 00 00	8.702	12 00 00	5.536	20 00 00	12.905
04 30 00	8.648	12 30 00	5.589	20 30 00	13.555
05 00 00	8.465	13 00 00	5.679	21 00 00	12.547
05 30 00	8.141	13 30 00	5.778	21 30 00	11.141
06 00 00	7.772	14 00 00	5.897	22 00 00	9.839
06 30 00	7.307	14 30 00	6.026	22 30 00	8.823
07 00 00	6.902	15 00 00	6.185	23 00 00	8.235
07 30 00	6.512	15 30 00	6.331	23 30 00	7.924

<sup>†</sup>For error bars see Table 12

Table 12. Accuracy of the absolute values of  $T_{sky}$  measured by TRIS at  $\delta = +42^\circ$

$\nu$ (GHz)	0.60	0.82	2.5
<i>statistical uncertainty</i>			
stand. dev. $\sigma$ (mK)	104	160	25
mean stand. dev. $\sigma_m$ (mK)	18	32	10
<i>systematic uncertainty</i>			
zero level (mK)	66	$^{+430}_{-300}$ <sup>†</sup>	284
polarization effect	< 2%	< 3%	< 2%

<sup>†</sup>See section 5.

Table 13. Accuracy of measurements in literature of  $T_{CMB}$  and  $T_{sky}$  at frequencies close to 0.6, 0.82 and 2.5 GHz

$\nu$ (GHz)	$\lambda$ (cm)	$\sigma_{sky}$ (K)	$T_{CMB}$ (K)	$\sigma_{CMB}$ (K)	Reference
0.610	49.1	0.7	3.7	1.2	1
0.6	50.0	0.9	3.0	1.2	2
0.635	47.2	$\sim 0.5$	3.0	0.5	3
0.82	36.6	1.5	2.7	1.6	4
2	15	$\leq 0.3$	2.5	0.3	5
2	15	0.10	2.55	0.14	6
2.3	13.1	0.2 - 0.4	2.66	0.7	7
2.5	12	0.15	2.5	0.21	4

References. — (1) Howell & Shakeshaft 1967; (2) Sironi et al. 1990; (3) Stankevich et al. 1970; (4) Sironi et al. 1991; (5) Pelyushenko & Stankevich 1969; (6) Bersanelli et al. 1994; (7) Otoshi & Stelzried 1975

Table 14. TRIS results summary

0.6 GHz	$\alpha^1 = 10^h00^m$	$\alpha^2 = 20^h24^m$
$T_{sky}$ (K)	$9.390 \pm 0.066$ ( <i>syst</i> ) $\pm 0.018$ ( <i>stat</i> )	$28.190 \pm 0.066$ ( <i>syst</i> ) $\pm 0.018$ ( <i>stat</i> )
$T_{gal}$ (K)	$5.72 \pm 0.07$	$24.44 \pm 0.07$
$T_{UERS}$ (K)		$0.934 \pm 0.024$
$T_{CMB}$ (K)		$2.823 \pm 0.066$ ( <i>syst</i> ) $\pm 0.129$ ( <i>MC</i> <sup>†</sup> )
$T_{CMB}^{th}$ (K)		$2.837 \pm 0.066$ ( <i>syst</i> ) $\pm 0.129$ ( <i>MC</i> <sup>†</sup> )
0.82 GHz	$\alpha^1 = 10^h00^m$	$\alpha^2 = 20^h24^m$
$T_{sky}$ (K)	$5.37_{-0.30}^{+0.46}$ ( <i>syst</i> ) $\pm 0.03$ ( <i>stat</i> )	$13.57_{-0.30}^{+0.46}$ ( <i>syst</i> ) $\pm 0.03$ ( <i>stat</i> )
$T_{gal}$ (K)	$2.21 \pm 0.03$	$10.38 \pm 0.03$
$T_{UERS}$ (K)		$0.408 \pm 0.010$
$T_{CMB}$ (K)		$2.783_{-0.300}^{+0.430}$ ( <i>syst</i> ) $\pm 0.051$ ( <i>MC</i> <sup>†</sup> )
$T_{CMB}^{th}$ (K)		$2.803_{-0.300}^{+0.430}$ ( <i>syst</i> ) $\pm 0.051$ ( <i>MC</i> <sup>†</sup> )
2.5 GHz	$\alpha^1 = 10^h00^m$	$\alpha^2 = 20^h24^m$
$T_{sky}$ (K)	$2.57 \pm 0.28$ ( <i>syst</i> ) $\pm 0.10$ ( <i>stat</i> )	$2.99 \pm 0.28$ ( <i>syst</i> ) $\pm 0.10$ ( <i>stat</i> )
$T_{gal}^{\dagger\dagger}$ (K)	$0.091 \pm 0.093$ ( <i>syst</i> ) $\pm 0.005$ ( <i>stat</i> )	$0.471 \pm 0.093$ ( <i>syst</i> ) $\pm 0.027$ ( <i>stat</i> )
$T_{UERS}$ (K)		$0.022 \pm 0.001$
$T_{CMB}$ (K)		$2.458 \pm 0.284$ ( <i>syst</i> ) $\pm 0.139$ ( <i>stat</i> )
$T_{CMB}^{th}$ (K)		$2.516 \pm 0.284$ ( <i>syst</i> ) $\pm 0.139$ ( <i>stat</i> )

<sup>†</sup>This uncertainty was evaluated by means of MonteCarlo simulations, as described in Paper II.

<sup>††</sup>Due to the incompleteness of the TRIS drift scan at 2.5 GHz, here  $T_{gal}$  is extrapolated by (Reich & Reich 1986) map at 1.42 GHz convolved with TRIS beam and using local spectral index calculated from our data at 0.6 and 0.82 GHz. The quoted systematic uncertainty for  $T_{gal}$  is relative to the determination of the galactic signal at 1.42 GHz, starting from the absolute measurements at 0.6 and 0.82 GHz.